Journal of Molecular Liquids 356 (2022) 119002

Contents lists available at ScienceDirect

Journal of Molecular Liquids

journal homepage: www.elsevier.com/locate/molliq

Elucidation of corrosion inhibition property of compounds isolated from Butanolic Date Palm Leaves extract for low carbon steel in 15% HCl solution: Experimental and theoretical approaches

Saviour A. Umoren [a,*], Rami K. Suleiman [a], Ime B. Obot [a], Moses M. Solomon [b], Akeem Y. Adesina [a]

[a] Interdisciplinary Research Center for Advanced Materials, King Fahd University of Petroleum and Minerals, Dhahran 31261, Saudi Arabia
[b] Department of Chemistry, College of Science and Technology, Covenant University, Ota, Nigeria

ARTICLE INFO

Article history:
Received 24 December 2021
Revised 14 February 2022
Accepted 22 March 2022
Available online 26 March 2022

Keywords:
Date palm
Acid corrosion
Isolation
Oleanolic acid
Vanillyl alcohol
Monte Carlo simulations

ABSTRACT

The present work reports on the corrosion inhibition property of compounds isolated from butanolic extract of Date Palm leaves for low carbon steel in 15% HCl solution. Six compounds were isolated from Date Palm leaves and purified using a combination of column chromatography, thin layer chromatography, and Prep HPLC-MS system. The isolated compounds were characterized using ^{1}H NMR, ^{13}C NMR, and GC–MS. Their identity was revealed to be a mixture of fatty alkanes, oleanolic acid (OA), vanillyl alcohol (VA), β-Sitosterol-3-O-β-D-glucoside (β-SSG), sucrose sugar, and carotenoid lutein. As a result of the amount of the different isolates obtained, only three out of the six compounds namely β-SSG, OA, and VA were tested for anticorrosion property for low carbon steel in 15% HCl. The corrosion inhibition of the isolated compounds was performed using weight loss and electrochemical techniques. Surface morphology analysis of the corroded steel in the absence and presence of the isolated compounds was undertaken using SEM/EDAX and 3D optical profilometer. Also, DFT calculations was performed in order to indicate the reactivities and bonding sites of the isolated molecules as well as Monte Carlos simulations (MCS) to determine the energy of interaction between the inhibitors and carbon steel surface. Results obtained show that the values of inhibition efficiency (IE) for the different isolated compounds at the concentration (35 ppm) studied follow the trend: β-SSG (46.57%) > $VA_{isolated}$ (39.30%) > $VA_{commercial}$ (36.81%) > OA (31.94%) at 25 °C. It is also noted that, for the isolated OA, IE increased with increase in concentration but decreased with increase in temperature. For isolated VA, IE decreased with increase in temperature. However, for the commercial VA, IE slightly increased with rise in temperature. The experimental results are in agreement with the theoretical prediction. In both predicted and experimental results, β-SSG is the best corrosion inhibitor.

1. Introduction

Corrosion is a material damage caused by chemical, electrochemical, and biological reactions. The global estimate for corrosion cost is in the region of US$ 2.5 trillion. Effective control strategies could lead to huge savings of between 15 and 35% of the yearly cost of corrosion deterioration [1]. One of the best strategies for combating corrosion is the use of corrosion inhibitors, which act by adsorbing themselves on the metallic surface, forming a thin film over the metal surface and hence protecting the metal from the aggressive anions present in the corrosive medium [2–10]. However, most of the inhibitors used in industries are composed of compounds like propargyl alcohol that are toxic; thus, they are facing criticism owing to their threat to humans and the environment. Consequently, the use of less toxic and renewable products as corrosion inhibitors is at the forefront of current research interest. The use of natural products as corrosion inhibitors has been advocated because they are renewable, readily available, ecologically acceptable, environmentally friendly, and inexpensive and can be obtained by simple extraction procedures [11,12]. Many researchers have therefore reported the inhibition of metal corrosion using plant extracts as green inhibitors [2–6].

The primary criticisms on the use of biomass extracts of plant origin as corrosion inhibitors is the inability to determine the specific component(s) that is/are responsible for the inhibition of corrosion because plant extracts are composed of mixtures of organic compounds. In an attempt to solve this problem, the current trend in research using plant extracts is to isolate the compo-

* Corresponding author.
E-mail address: umoren@kfupm.edu.sa (S.A. Umoren).

https://doi.org/10.1016/j.molliq.2022.119002
0167-7322/

nents and investigate the corrosion inhibition potential of each component or, alternatively, to test pure compounds of the identified principal/active component(s) along with the crude plant extract. Studies on the use of crude plant extracts together with pure compounds of their principal/active component(s) as corrosion inhibitors for mild steel in acidic environments have been published. For example, Garai *et al.* [13] reported that Arbutin, an active component from *Artemesia pallens*, and the crude methanolic extract of this plant exhibited inhibition efficiencies of 93% and 98%, respectively, at a concentration of 400 mg L^{-1} at 30 °C for mild steel in a 1 M HCl solution. Li *et al.* [14] reported that bamboo leaf extract and two major components from the extract, rutin and orientin, acted as moderate inhibitors for the corrosion of cold rolled steel in a 0.1 M H_3PO_4 solution. The inhibition efficiency of these substances was in the following order: leaf extract (51.2%) > rutin (42.5%) > orientin (34.0%) at a 100 mg L^{-1} concentration at 25 °C. The inhibitory effect of *Neolamarckia cadamba* crude extract (bark and leaves) and a pure alkaloid (3β-isodihydrocadambine) isolated from the extract on mild steel corrosion in a 1 M HCl medium had also been investigated [15]. The results showed that the crude extracts and 3-β-isodihydrocadambine significantly reduced the corrosion rate of the metal at all of the concentrations tested. The effect of an extract of *Punica granatum* (PG) and its primary constituents, ellagic acid (EA) and tannic acid (TA), as mild steel corrosion inhibitors in 2 M HCl and 1 M H_2SO_4 solutions investigated by weight loss measurements had been reported [16]. It was found that the PG peel extract and EA inhibited the corrosion of mild steel in 2 M HCl and 1 M H_2SO_4, but the efficiency was slightly better in the HCl solution than in H_2SO_4. Kamal and Sethuraman [17] have reported that the anticorrosion potential of a marine alga *Caulerpa racemosa* against mild steel in a 1 M HCl solution can be correlated to caulerpin (a bis-indole alkaloid). Isoreserpiline and other alkaloids extracted from the leaves and bark of *Ochrosia oppositifolia* have been investigated as potential corrosion inhibitors for mild steel in a 1 M HCl solution [18]. All of the samples tested (leaves, bark and isoreserpiline) displayed good inhibition properties and showed excellent performance (more than 85% at 20–25 mg L^{-1}) as corrosion inhibitors. Fourier transform infrared (FTIR) spectroscopy and molecular modeling studies revealed that isoreserpiline is most likely responsible for the corrosion inhibition potential of *Ochrosia oppositifolia* extract. Similarly, the inhibitory action of henna (*Lawsonia inermis*) extract and its primary constituents (lawsone, gallic acid, α-D-Glucose and tannic acid) on the corrosion of mild steel in a 1 M HCl solution had been evaluated by Ostovari *et al.* [19]. The results showed that all of the examined henna constituents acted as mixed-type inhibitors for the corrosion of mild steel in 1 M HCl with good inhibition efficiencies in the following order: lawsone > gallic acid > α-D-Glucose (dextrose) > tannic acid. The primary constituent responsible for the inhibitory characteristics of henna extract was lawsone. The corrosion inhibitory effect of *Aniba rosaeodora* alkaloid extract on C38 carbon steel in 1 M HCl has been reported [20]. Anibine was found to be the major alkaloid present in the extract from studies of the phytochemical constituents and was responsible for the observed corrosion inhibition efficiency of the total extract. Recently, andrographolide, a bioactive naturally occurring labdane diterpenoid was isolated, purified from *Andrographis paniculata*, and investigated as a corrosion inhibitor for carbon steel in acid-chloride environments. Results obtained revealed that andrographolide is an effective mixed type corrosion inhibitor with optimum inhibition efficiency of 92.4% at the inhibitor concentration of 2 g/L after 48 h immersion at 45 °C [21].

In our previous communications, we reported that Date Palm leaves extract is a promising corrosion inhibitor [22–25]. We noted that, of acetone, ethanol, aqueous, butanol, methanol, isopropanol, and ethyl acetate used as the extracting solvent, the butanolic extract exhibited the best corrosion inhibition performance for carbon steel in 15% HCl solution [24]. At a concentration of 1000 ppm, the butanolic extract afforded 97 and 86% protection at 25 and 60 °C, respectively. This finding raised some pertinent questions such as: why is butanolic extracts performing better and which compound(s) is/are responsible for it? The present study was therefore designed to provide answers to these questions. Herein, we report on the isolation and characterization of some bioactive compounds present in butanolic Date Palm extract and their corrosion inhibition potential for X60 carbon steel in 15% HCl solution. The corrosion inhibition study was performed using electrochemical techniques (EIS and PDP) and weight loss method at 25 and 60 °C complemented by surface morphology analysis of the corroded steel specimen without and with the different isolates with SEM/EDAX and 3D optical profilometer. Also, Monte Carlos simulations — a powerful tool for studying interactions between adsorbates and substrates at the microscopic level was utilized to gain more understanding of the mechanisms of interaction between some of the isolated compounds from the butanolic extract and the steel surface at the molecular level.

2. Experimental

2.1. Materials and chemicals

The Date Palm leaves were collected from the KFUPM campus, Dhahran, Saudi Arabia in the month of May 2020. The identification and validation of the leaves were handled by Dr. Jacob Thomas of King Saud University, Riyadh, Saudi Arabia and the leaves specimen has been deposited in the King Saud University herbarium with KSU No. 22638 as the identification number. The leaves were cut into smaller pieces, washed with distilled water, sun dried for one week, and ground into powder. All the chemicals used in the extraction and column chromatography (CC) procedures were of analytical grade. They were procured from Sigma-Aldrich Company (USA) and used as received without further purification. HPLC-grade solvents and a 0.45 μm-filtered distilled water was used in the preparation of the mobile phase for the LC-MS analysis. The chemical composition of the X60 carbon steel is as previously reported [26]. The procedure adopted in sample surface treatment was as listed in ASTM G1-90 procedure [27]. Mechanical grinding of the metal sample was carried out using Buchler CarbiMet™ papers of different grit sizes progressively from 120 to 1000. The corrosive medium was 15 wt% HCl solution prepared by diluting appropriate amount of analytical grade hydrochloric acid (37%, Merck) with double distilled water.

2.2. Extraction, isolation, and identification of bioactive compounds

The finely powdered Date Palm leaves (140 g) were extracted with butanol in a 1:3 (powder: solvent) ratio in a 1 L beaker with continuous stirring at 500 rpm and 25 °C for 48 h. The crude butanolic extract was filtered through double Whatman No. 1 filter papers and concentrated by evaporation under decreased pressure over a water bath at 60 °C to obtain 60 g of dark greenish extract. This extract was purified using column chromatography (CC) with ethyl acetate as the eluent and increasing polarity with methanol, yielding seven fractions (F1-F7). Column chromatography was used to further purify fractions F2 and F4. The addition of methanol to F1 resulted in a 51.6 mg pure white solid that was identified as a combination of fatty alkanes (tetracosane, pentacosane, hexacosane, heptacosane, and octacosane) by NMR and GC–MS (Fig. 1 (e)). Fraction F2 (9.5 g) was purified further using CC with hexane as the eluent and increasing polarity with ethyl acetate and then methanol to get 5 fractions based on TLC performance. Subfraction

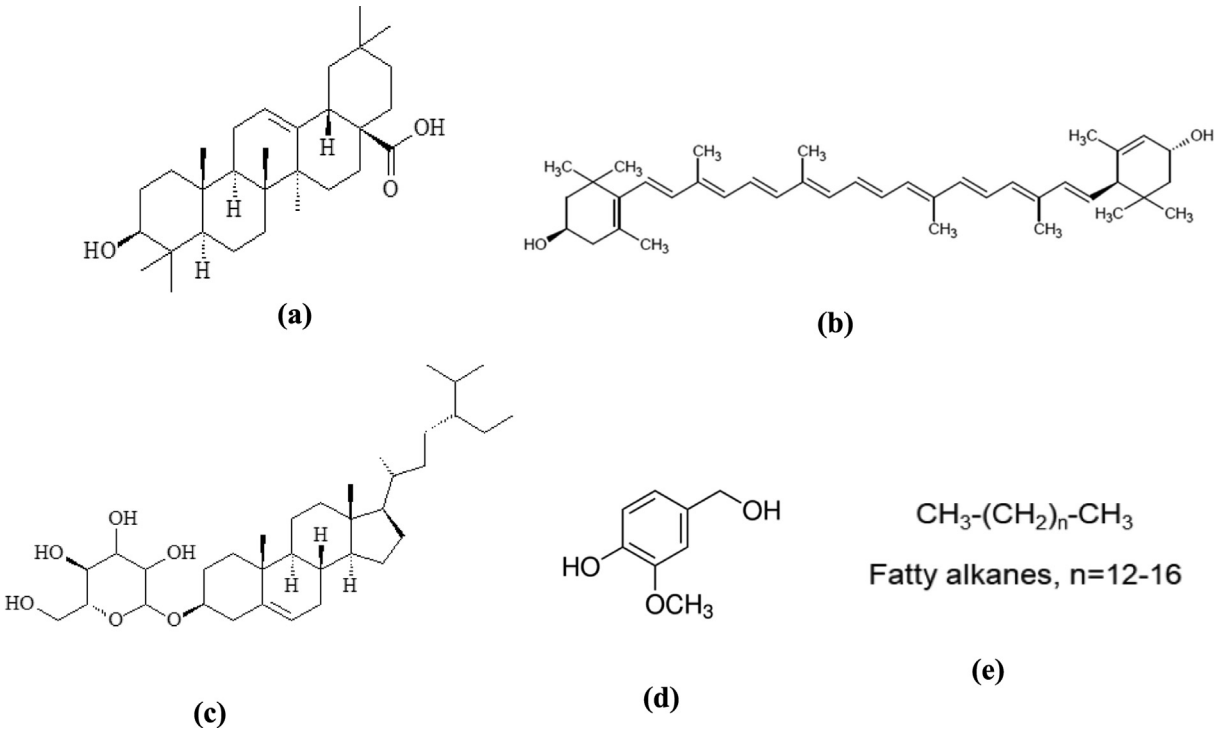

Fig. 1. Chemical structures of some of the isolated compounds from date palm butanolic extract (a) Oleanolic acid (OA), (b) Lutein, (c) β-Sitosterol-3-O-β-D-glucoside (β-SSG), (d) Vanniyl alcolol (VA) and (e) Fatty alkanes.

F2-2 yielded a UV-inactive chemical, which was refined further with methanol to obtain 217.7 mg white solid, which was identified as oleanolic acid (Fig. 1(a)). F2-4 had a dark yellow spot on TLC that was identified as the pigment lutein by LC-MS analysis. The addition of methanol to F3 and Subfraction F2-5 yielded 373.7 mg of vanillyl alcohol, a UV-active molecule (Fig. 1(d)). F4 revealed a substantial UV-inactive molecule (pink color spot on TLC after spraying with anisaldehyde TLC visualization reagent), which was purified further with methanol to yield 9.2 mg of β-Si tosterol-3-O-β-D-glucoside (Fig. 1(c)). Finally, after adding methanol to F5, a 20 mg translucent substance identified as natural sugar sucrose was obtained.

The isolates were identified and characterized using high-resolution ^{1}H and ^{13}C NMR spectra recorded at 500 and 128 MHz, respectively, using a Bruker Avance 400 MHz spectrometer. The samples were dissolved in $CDCl_3$ or DMSO d_6, and the chemical shifts were measured in parts per million (ppm) using tetramethylsilane (TMS) as an internal reference. A ISQTM 7000 Single Quadrupole GC–MS System was used for the GC–MS analysis (ThermoFisher Scientific). A TraceGOLD TG-5MS GC capillary column (5% phenyl and 95% dimethyl polysiloxane) with 30 m × 0.25 mm × 0.25 μm dimensions is included with the instrument. The Agilent 1200 series LCMS-6120B coupled with a Diode-Array Detector (DAD) and a Poroshell 120 EC-C18 (4.6 × 15 0 mm, 4 μm) column was used for the LC-MS analysis. The column oven was kept at a constant temperature of 25 °C. The analysis was performed using isocratic elution with a mobile phase of 0.1% formic acid in water (solution A, 80%) and methanol (solution B, 20%); post-time was 5 min before the next injection. The mobile phase flow rate was 1.0 mL/min, and the sample injection volumes were 20 μL.

2.3. Corrosion inhibition evaluation of the isolated compounds

Corrosion inhibition performance of the isolated compounds was assessed utilizing electrochemical and weight loss methods. Electrochemical experiments were performed utilizing the conventional three-electrode cell assembly. A platinum wire and silver/silver chloride electrode (Ag/AgCl) were employed as counter and reference electrode respectively. The X60 steel serves as the working electrode with an exposed surface area of 1 cm^2. The polarization and impedance measurements were conducted using VERSASTAT 3 (Princeton Applied Research, USA) electrochemical workstation at room temperature, in an open air. Before commencement of each measurement, the electrode was immersed in each test solution for 3600 s to attain the steady-state open circuit potential (E_{OCP}). The potentiodynamic polarization curves were recorded by sweeping the potential from cathodic to anodic direction with respect to the open circuit potential (−250 mV to +250 mV) at a sweep rate of 0.5 mV/s. The corrosion current density I_{corr} and the corrosion potential E_{corr} were obtained by extrapolation of Tafel lines. The impedance measurements were conducted at OCP in the frequency range 100,000 Hz to 0.01 Hz, with an amplitude of 10 mV peak to peak. The impedance measurement experiments were repeated thrice for reproducibility. Electrochemical parameters of interest were obtained from the impedance measurements by analyzing the experimental data with Zsimpwin software.

The influence of temperature on the corrosion inhibition efficacy of the different isolates was evaluated using weight loss measurement. The experiment was carried out in glass reaction vessels containing 250 mL of test solution that were kept at 25 and 60 °C with a thermostated water bath. In the absence and presence of inhibitors, tests were carried out under whole immersion. Duplicate samples of the cleaned and weighed steel coupons were freely suspended in the various test solutions in each experiment. After a 24-hour immersion, the test coupons were removed, properly cleaned following standard procedures [27], rinsed with distilled water and acetone, dried in warm air, and reweighed using a digital analytical balance with a sensitivity of 0.1 mg. The difference between the initial weight (i.e the weight of the sample before immersion in test solution) and the final weight (i.e the weight

of the sample after immersion in the test solution for 24 h) was used to calculate the weight reduction. The average values of the triplicate determinations were reported because the results demonstrated good repeatability. Corrosion rates in terms of thickness loss (mm y^{-1}) were calculated based on the weight loss values using the expression:

$$C_R(\text{mm y}^{-1}) = \frac{87.6 \times \Delta W}{\rho A T} \quad (1)$$

where CR stands for corrosion rate, W for average weight loss (mg), ρ for X60 steel specimen density (g cm^3), A for specimen surface area (cm^2), and T for exposure period (h).

Equations (2) and (3) were used to calculate the surface coverage (θ) and the inhibition efficiency (IE), respectively.

$$\theta = \frac{C_{R(\text{blank})} - C_{R(\text{inh})}}{C_{R(\text{blank})}} \quad (2)$$

$$IE = \frac{C_{R(\text{blank})} - C_{R(\text{inh})}}{C_{R(\text{blank})}} \times 100 \quad (3)$$

where $C_{R(blank)}$ and $C_{R(inh)}$ are the corrosion rate in the absence and presence of the inhibitor respectively in 15% HCl at 25 °C or 60 °C.

2.4. Surface morphology analysis

A JEOL JSM-6610 LV scanning electron microscope (SEM) was used to examine the surface morphology of the X60 steel specimens without and with the isolated compounds in the acid medium after 24 h exposure. The pre-cleaned coupons were immersed for 24 h in 15% HCl solution without and with 200 ppm OA and VA at 25 ± 1 ∘C as well as 200 ppm VA at 60 °C, and then rinsed with distilled water, dried in warm air, and submitted for SEM surface examination. The surface roughness of the exposed area of the steel coupons immersed in the solution without and with the isolates was measured using a 3D optical profilometer (Contour GT-K, Bruker Nano GmBH, Germany).

2.5. Theoretical studies

2.5.1. Density functional theory (DFT) calculations

Quantum chemical calculations based on DFT method was employed. Becke exchange functional and the Lee Yang Parr correlation functional (BLYP), together with the generalized gradient approximation (GGA) employing the "double numeric polarization" (DNP) basis sets was used in optimization of the geometries of OA, β-SSG and VA molecules. Double Numerical plus polarization include a polarization p-function on all hydrogen atoms. It has best accuracy, but with highest computational cost. The calculation was carried out in the presence of water to simulate the effect of solvent since corrosion takes place in aqueous environments. In this case, the COSMO implicit solvent model using water and with dielectric constant of 78.54 was selected as the value for water. The convergence criteria and the global orbital cutoffs were set to "fine" before the calculations. The tolerances of energy, gradient, and displacement convergence were 1×10^{-5} Ha, 2×10^{-5} Ha. $Å^{-1}$ and 5×10^{-3} Å, respectively. Direct inversion in an iterative subspace (DIIS) and an orbital occupancy smearing parameter of 0.005 Ha were used to speed up the convergence.

2.5.2. Monte Carlo simulation

Metropolis Monte Carlo approach [28] using adsorption locator module in BIOVIA Materials studio 2019 was adopted to simulate the adsorption interaction of OA, β-SSG and VA molecules with the steel surface. The calculation was performed using the Condensed-phase Optimized Molecular Potentials for Atomistic Simulation Studies (COMPASS II) force field. The adsorption of the inhibitors was simulated on the Fe (1 1 0) crystal plane. The process involved cleaving from bcc Fe crystal, followed by enlargement to a (12 × 12) supercell and, thereafter, building of a 30 Å thick vacuum slab on the Fe (1 1 0). The adsorption energy for the most stable corrosion inhibitor–Fe (1 1 0) configuration was calculated by considering 200 molecules of water in order to account for the solvent effects. More information about the theory and methodology of Monte Carlo simulation can be found elsewhere [28–31].

3. Results and discussion

3.1. Isolation and characterization of bioactive compounds

Six compounds were isolated and purified from butanolic Date Palm leaves extract using a combination of column chromatography, thin layer chromatography and Prep HPLC-MS system. The isolated compounds were characterized using ^{1}H NMR ^{13}C NMR and GC–MS. Their identity was revealed to be mixture of fatty alkanes, oleanolic acid (OA), vanillyl alcohol (VA), β-Sitosterol-3-O-β-D-glucoside (β-SSG), sucrose sugar and carotenoid lutein. Chemical structures of some of the isolated compounds are presented in Fig. 1. Detailed information on the isolation and characterization of the bioactive compounds could be found in our earlier publication [32]. However, on the basis of the amount extracted, OA, VA, and β-SSG were selected for anticorrosion studies as the other three were extracted in minute amount.

3.2. Corrosion inhibition evaluation of the isolates

3.2.1. OCP and EIS measurements

Fig. 2(a) shows the variation of open circuit potential (E_{OCP}) with immersion time for X60 carbon steel in 15% HCl solution without and with 35 ppm of the different isolates at 25 °C. Inspection of the plots reveals that at least a pseudo-stability was achieved for both uninhibited and inhibited systems within the chosen 3600 s delayed time. However, a close inspection of the graphs (both uninhibited and inhibited) reveals that, upon the commencement of the measurement, the E_{OCP} progresses in a positive direction until a pseudo stable condition was reached. Such progression, which had been previously reported [33] is associated with the premier corrosion process of the pre-exposure, air-formed oxide layer, and the initial attack on the substrate surfaces. When the E_{OCP} vs time graph of the blank is compared to those of the inhibited, it is seen that the E_{OCP} is displaced anodically, that is, the E_{OCP} of the uninhibited system is nobler relative to the E_{OCP} of the inhibited systems. This may point to the preferential adsorption of the isolates on the anodic sites of the X60 carbon steel interface [34]. Nevertheless, the displacement placed the isolates in the category of mixed-type inhibitors as it is not up to the benchmark of +85 mV/Ref required for the categorization of an inhibitor as anodic- or cathodic-type [34,35].

To evaluate the corrosion inhibiting potentials of the isolates, the impedance characteristics of X60 steel in 15% HCl solution with and without 35 ppm concentration of the isolates (β-SSG, VA, OA) at 25 °C was collected. The recorded impedances in Nyquist and Bode formats are presented in Fig. 2. In all cases, the Nyquist plots (Fig. 2(a)) exhibit a capacitive loop in the high-to-medium frequency range and a poorly developed inductive loop at the low frequency range. Generally, the capacitive loop is associated with a charge transfer process [36,37] while the inductive loop could be linked to the relaxation of adsorbed corrosion products and/or adsorbed inhibitor films on the metal surface [38]. Meanwhile, for the semi-circles obtained for the isolates inhibited systems

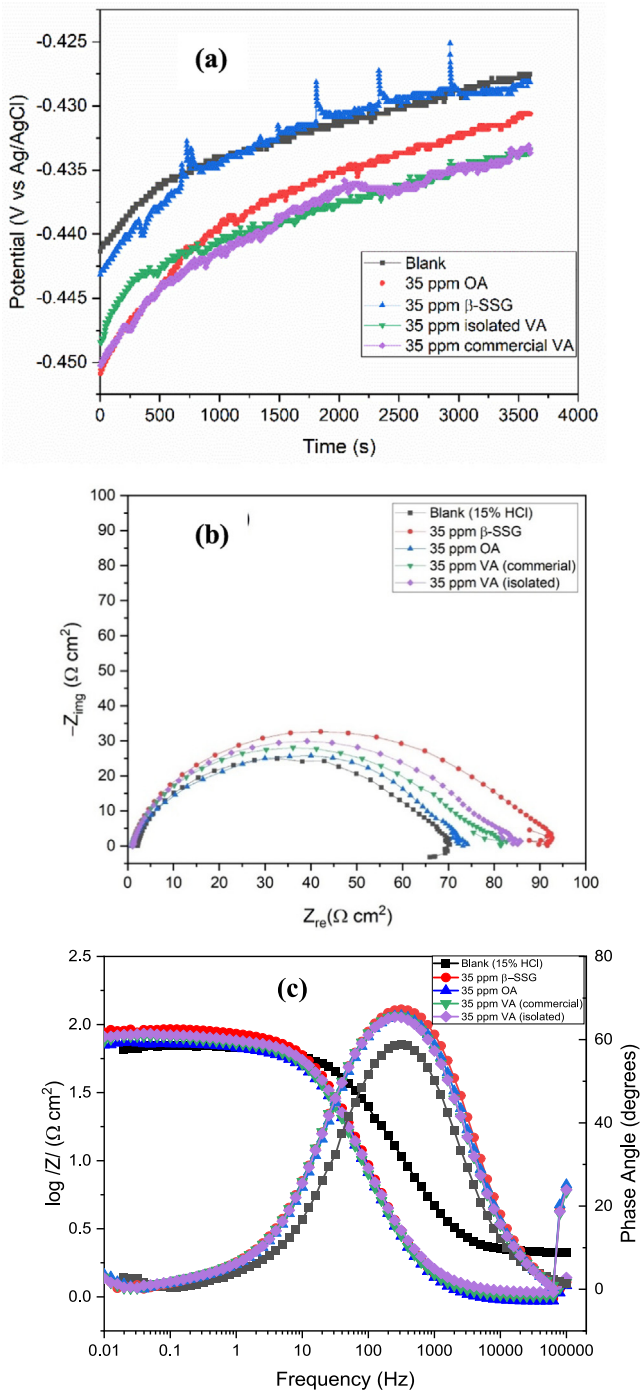

Fig. 2. (a) Variation of open circuit potential with immersion time for X60 carbon steel in 15% HCl solution without and with 35 ppm of the different isolates at 25 °C; Impedance plots for X60 carbon steel in 15% HCl solution without and with 35 ppm of the different isolates at 25 °C (b) Nyquist and (c) Bode formats.

(Fig. 2(a)), the diameter of the capacitive loop is larger than that of the blank. The inhibiting effect of the isolates can as well be seen in the Bode graphs (Fig. 2(b)). This implies that the presence of the isolates in the acid solution improved the corrosion resistance property of the carbon steel. That is, the studied isolates acted as inhibitor for carbon steel corrosion in 15% HCl solution. However, the inhibiting effect of the isolates varies (Fig. 2) and follow the order: β-SSG > VA > OA. This could be due to the differences in the adsorption groups in the isolates and poor solubility property of OA in the selected solvent. The Density Functional Theory calculation and Monte Carlo simulations shall be used later to gain more insight into the observation. It is worthy to mention that prior to introducing the isolated compounds into the corrosive medium (15% HCl), each concentration of the isolates (35 ppm β-SSG, VA, OA) was dissolved in a small amount of DMSO (dimethyl sulfoxide). This was necessary as the isolates were not soluble in aqueous medium. However, while β-SSG and VA exhibited good solubility in DMSO, OA was sparingly soluble.

The analysis of the electrochemical data was accomplished using the electrical equivalent circuit (EC) shown in Fig. 3(a). The fitted impedance for VA, β-SSG, and OA are shown in Fig. 3(b-d). The suitability of the selected EC is also reflected in the low x^2 values as listed in Table 1(a). The components of the EC include solution resistance (R_s), charge transfer resistance (R_{ct}), constant phase element (CPE), and film resistance (R_f). The constant phase element (Z_{CPE}) is defined by Equation (4) [39]:

$$Z_{CPE} = Y^{-1}(jw)^{-n} \tag{4}$$

where Y is the CPE constant, n is the CPE exponent, a parameter that can be used to determine the heterogeneity of a surface, j is an imaginary number, and w the angular frequency in rad. s^{-1} [24]. The results from the analysis are presented in Table 1(a). The C_{dl} was calculated using the Brug's formula [40] (Eq. (5)) while the percentage inhibition efficiency (%IE) was computed making use of Eq. (6) [23].

$$C_{dl} = {Y_{dl}}^{1/n_{dl}} \left(\frac{1}{R_s} + \frac{1}{R_{ct}}\right)^{(n_{dl}-1/n_{dl})} \tag{5}$$

$$\mathrm{IE} = \left(\frac{\mathrm{R_{total\ \ inhibited}} - \mathrm{R_{total\ \ blank}}}{\mathrm{R_{total\ \ inhibited}}}\right) \times 100 \tag{6}$$

The derived and the calculated parameters are given in Table 1 (a). It is obvious from the Y_{dl} and Y_f values given in Table 1(a) that the studied isolates adsorb on the metal surface and form a surface film with superior property than the corrosion product on the uninhibited metal surface. The smaller Y_{dl} and Y_f values for the β-SSG, VA, OA surfaces compared to that of the unprotected surface is indicative of a surface film with better characteristics [40]. The C_{dl} value reveals a thicker surface film on the protected surfaces than in the unprotected, that is, the decrease in the C_{dl} values of the protected surfaces relative to the unprotected is due to increase in the thickness of the adsorbed surface film [40]. The adsorption of β-SSG, VA, and OA on the carbon steel surface led to an increase in the polarization resistance from 53.84 Ω cm^2 to 100.77 Ω cm^2, 79.11 Ω cm^2, and 88.70 Ω cm^2, respectively amounting to 46.57%, 31.94%, and 39.30% protection against corrosion. As earlier noted, β-SSG exhibit the best inhibition ability.

One of the challenges during corrosion inhibitor formulation is the selection of a suitable solvent. Solvent selection is an important factor as it directly affects the inhibition performance of an inhibitor [25,41]. An inhibitor that is soluble or highly dispersible in its environment of application exhibits better inhibiting effect than an inhibitor that is poorly soluble. As previously mentioned, OA exhibited poor solubility property in DMSO relative to other isolates (β-SSG and VA). It was therefore essential to identify a suitable solvent for OA. To demonstrate that increasing the concentration of an inhibitor in a wrong solvent is not an option, 35 and 200 ppm of OA were prepared in DMSO while 100 ppm OA was prepared in DMF (dimethylformamide). OA is highly soluble in DMF. The impedance plots for X60 carbon steel in 15 wt% HCl solution without and with 35 ppm, 100 ppm, and 200 ppm concentrations of OA at 25 °C is given in Fig. 4 and the corresponding derived data are summarized in Table 1(b). As could be seen in Fig. 4 and Table 1(b), although there is a slight improvement in corrosion inhibition effect of OA as the concentration was increased

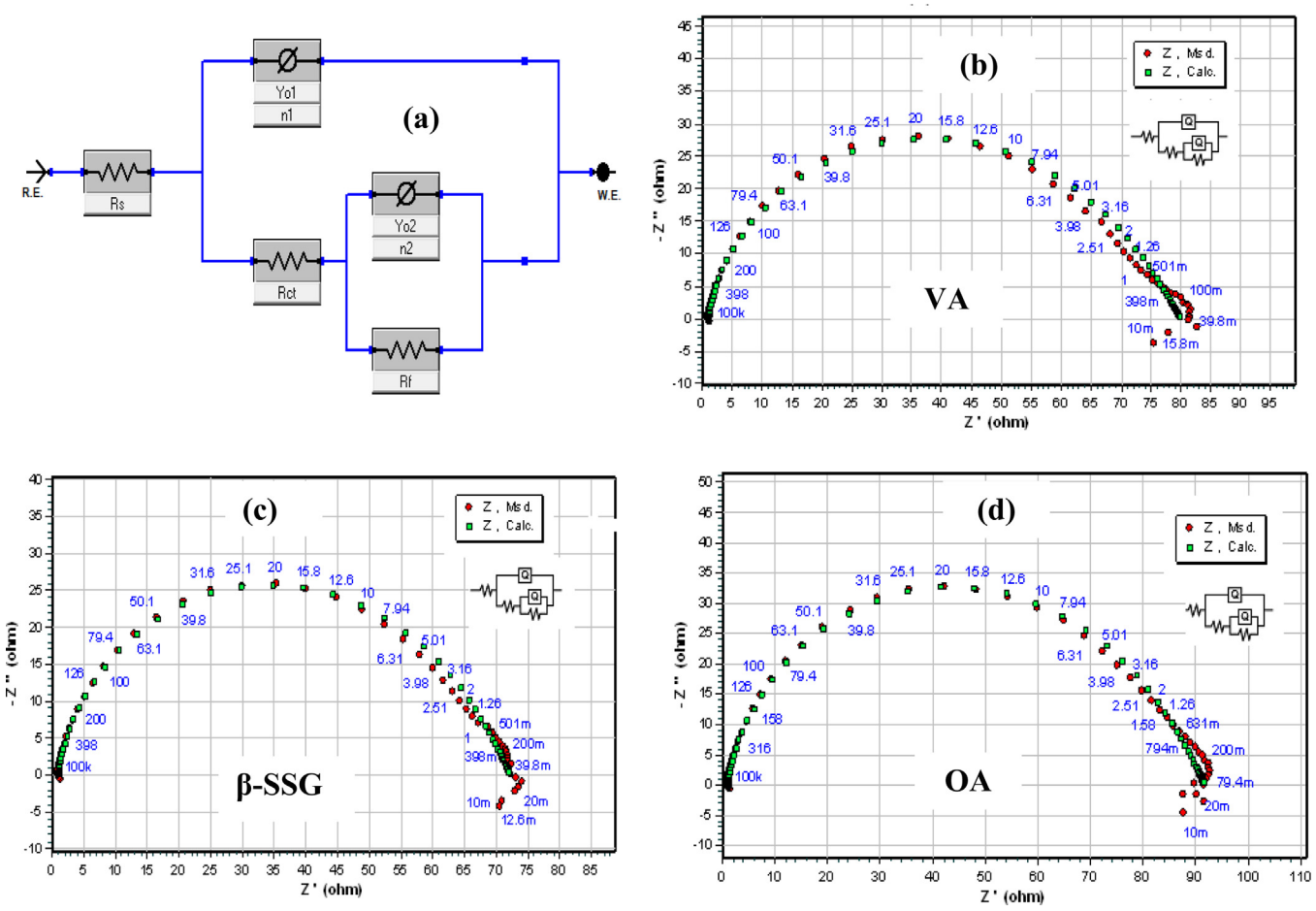

Fig. 3. (a) Equivalent circuit used to fit the experimental data. The fitted impedance for VA, β-SSG, and OA are shown in (b), (c), and (d), respectively.

Table 1a
EIS parameters obtained during acid corrosion of X60 carbon steel in 15% HCl solution without and with 35 ppm of different isolates at 25 °C.

Conc. (ppm)	R_s (Ω cm^2)	CPE_{dl}		R_{ct} (Ω cm^2)	CPE_f		R_f (Ω cm^2)	(R_p = R_f + R_{ct}) (Ω cm^2)	C_{dl} (μFcm^{-2})	$\chi^2(\times10^{-4})$	%IE
		Y_{dl} (μFcm^{-2} s^{n-1})	n_{dl}		Y_f (μF cm^{-2} s^{n-1})	n_f					
Blank	1.54	277.60	0.86	46.90	8624.0	0.89	6.94	53.84	78.1	3.38	–
β-SSG	1.06	53.00	1.00	90.73	324.9	0.63	10.04	100.77	53.0	102.0	46.57
OA	1.01	61.70	1.00	71.35	387.1	0.64	7.76	79.11	61.7	104.0	31.94
VA (Commercial)	1.08	61.49	1.00	78.84	430.2	0.62	6.37	85.21	61.5	87.9	36.81
VA (isolated)	1.17	55.23	1.00	82.21	351.0	0.64	6.49	88.70	55.2	90.4	39.30

from 35 ppm to 200 ppm, the 100 ppm dissolved in DMF shows a remarkable inhibitory performance. While 68.34% inhibition efficiency is achieved by dissolving 100 ppm OA in DMF, 44.69% is obtained with 200 ppm in DMSO. The poor performance of OA dissolved in DMSO is not unconnected with its poor solubility as it was visibly noted to precipitate on introduction into the corrosive medium meaning that the amount of the inhibitor available in the corrosive environment for adsorption onto the steel surface to inhibit corrosion was limited. On the other hand, OA dissolved in DMF was highly dispersible in the corrosive medium hence more of the inhibitor was available for adsorption onto the metal surface to inhibit corrosion.

Fig. 5 shows the comparative impedance plots for X60 carbon steel in 15% HCl solution containing either 35 ppm or 200 ppm of commercially available VA and the isolated VA at 25 °C in (a) Nyquist and (b) Bode plots. The quantitative data obtained from the analysis of the impedance data are listed in Table 1(c). The isolated VA at both concentrations (35 and 200 ppm) is found to perform slightly better than the commercially available VA. For instance, at 35 ppm, the inhibition efficiency of the commercially available VA is 36.81% while that of the isolated VA is 39.30%. The efficiency increased to 43.21% upon an increment in the concentration of the isolated VA to 200 ppm while that of the commercial VA decreased to 34.58%. It is a known fact that the property of plant phytocompounds is affected by its source, location, and even the extraction solvent and method [25,41].

3.2.2. Potentiodynamic polarization measurements

The polarization curves of X60 steel in 15% HCl solution at 25 °C in the absence and presence of various isolates of butanolic date

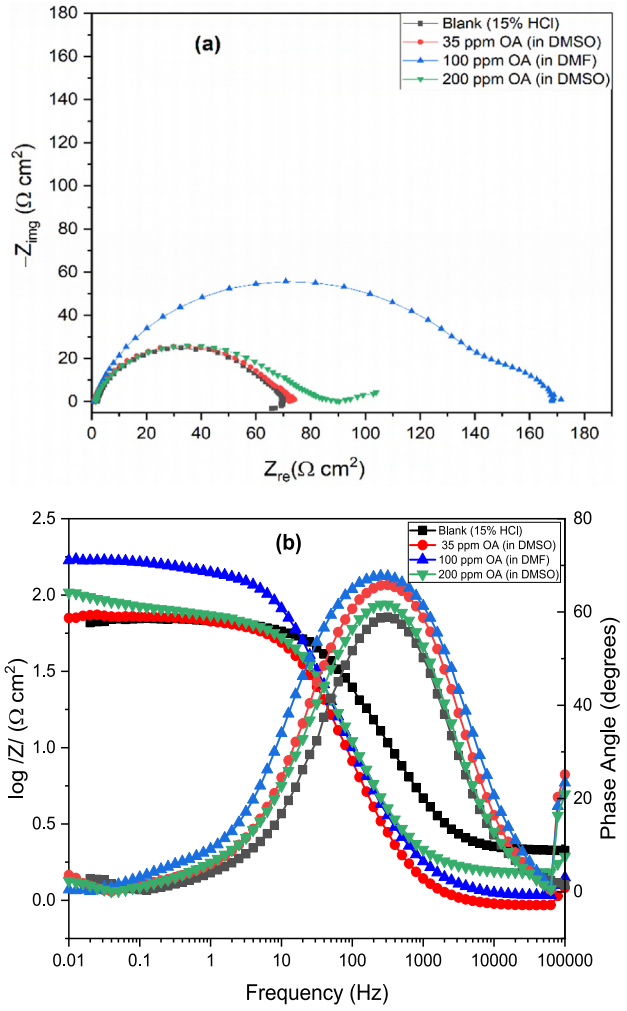

Fig. 4. Impedance plots for X60 carbon steel in 15% HCl solution without and with different concentrations of OA at 25 °C (a) Nyquist and (b) Bode plots.

palm leaf extract (β-SSG, OA, and VA) are shown in Fig. 6. The related electrochemical parameters, i.e., corrosion potential (E_{corr}), corrosion current density (i_{corr}), anodic Tafel slope (β_a), cathodic Tafel slope (β_c) and inhibition efficiency (IE) values are listed in Table 2. The inhibition efficiency (IE) was calculated following the equation:

$$IE = \left(1 - \frac{i_{corr}}{i^{o}_{corr}}\right) \times 100 \quad (7)$$

where i^{o}_{corr} and i_{corr} are the corrosion current densities in the absence and presence of inhibitors (isolates), respectively. Inspection of Fig. 6 and Table 2 reveals the following. (i) Relative to the E_{corr} of the blank, the presence of the isolates only causes a slight displacement, which is a common characteristic of a mixed-type corrosion inhibitor [42]. (ii) There is absent or near absent of diffusion-controlled mechanism resulting in a sufficient linear Tafel regions in the polarization curves. This justifies the suitability of Eq. (4) in the computation of the C_{dl}. Eq. (4) is derived for a system that diffusion process is not accounted for [40]. The fact that the cathodic branch obeys Tafel law indicates that the hydrogen reduction reaction on the surface of the low carbon steel in both unprotected and protected HCl solution proceeds according to a pure activation mechanism [43]. (iii) The addition of the isolates to the corrosive medium decreases both the cathodic and the anodic current densities and minimally modifies the cathodic and anodic Tafel slopes (β_c, β_a) (Fig. 6 & Table 2), again portraying the mixed-type characteristic of the isolates. However, a close inspection of Fig. 6 discloses that the presence of the isolates in the acid solution has a more pronounced effect on the cathodic reduction reaction. This implies that, although the isolates affected both the anodic and cathodic corrosion reactions, they have greater effect on the cathodic reduction reaction than anodic oxidation reaction. (iv) The anodic and the cathodic curves (Fig. 6) of both the uninhibited and inhibited are similar meaning that the anodic oxidation and the cathodic reduction reactions were not modified by the isolates in the process of inhibition. The observed inhibition may have involved the adsorption of the inhibitor molecules onto the carbon steel surface and the interference in the corrosion process via merely blocking the reaction sites on the carbon steel surface. In this way, the surface area available for corrosion decreased while the actual reaction mechanism remains unaffected. The active sites blocking mechanism can be justified by calculating the coefficients of anodic (f_a) and cathodic (f_c) reactions [44]. Interface inhibitors inhibit metals corrosion by active site blocking mechanism if f_a and f_c values are less than unity [44]. f_a and f_c can be computed using Eqs. (8) and (9) [24], respectively. As could be seen in Table 2, the calculated f_a and f_c values are less than unity and thus confirm that the inhibition of X60 steel corrosion in 15% HCl solution by β-SSG, OA, and VA is by active site blocking mechanism.

$$f_a = \left(\frac{i^{inhibited}_{corr}}{i^{blank}_{corr}}\right) e^{\frac{E^{blank}_{corr} - E^{inhibited}_{corr}}{\beta_a}} \quad (8)$$

$$f_c = \left(\frac{i^{inhibited}_{corr}}{i^{blank}_{corr}}\right) e^{\frac{E^{blank}_{corr} - E^{inhibited}_{corr}}{\beta_c}} \quad (9)$$

Worthy of mentioning is the comparative performance of the isolated compounds relative to the commercial and the outstanding inhibition performance of OA (DMF) compared to OA (DMSO) (Table 2). The results, which are in good agreement with the EIS results (Table 1) again underscore the importance of selecting the right solvent during the formulation of a corrosion inhibitor package.

3.2.3. Effect of temperature on corrosion inhibition

In order to assess the influence of temperature on the corrosion inhibition efficacy of the isolates particularly OA and VA, weight

Table 1b
EIS parameters obtained during acid corrosion of X60 carbon steel in 15% HCl solution without and with different of Oleanolic Acid (OA) at 25 °C.

Conc. (ppm)	R_s (Ω cm^2)	CPE_{dl}		R_{ct} (Ω cm^2)	CPE_f		R_f (Ω cm^2)	(R_p = R_f + R_{ct}) (Ω cm^2)	C_{dl} (μFcm^{-2})	x^2(×10^{-4})	%IE
		Y_{dl} (μFcm^{-2} s^{n-1})	n_{dl}		Y_f (μF cm^{-2} s^{n-1})	n_f					
Blank	1.54	277.60	0.86	46.90	8624.0	0.89	6.94	53.84	78.1	3.38	–
35 (DMSO)	1.01	61.70	1.00	71.35	387.1	0.64	7.76	79.11	61.7	104.0	31.94
100 (DMF)	1.18	40.67	1.00	163.8	315.8	0.63	6.25	170.05	40.7	98.5	68.34
200 (DMSO)	1.57	99.60	0.93	97.29	91.36	0.94	0.048	97.34	51.4	91.1	44.69

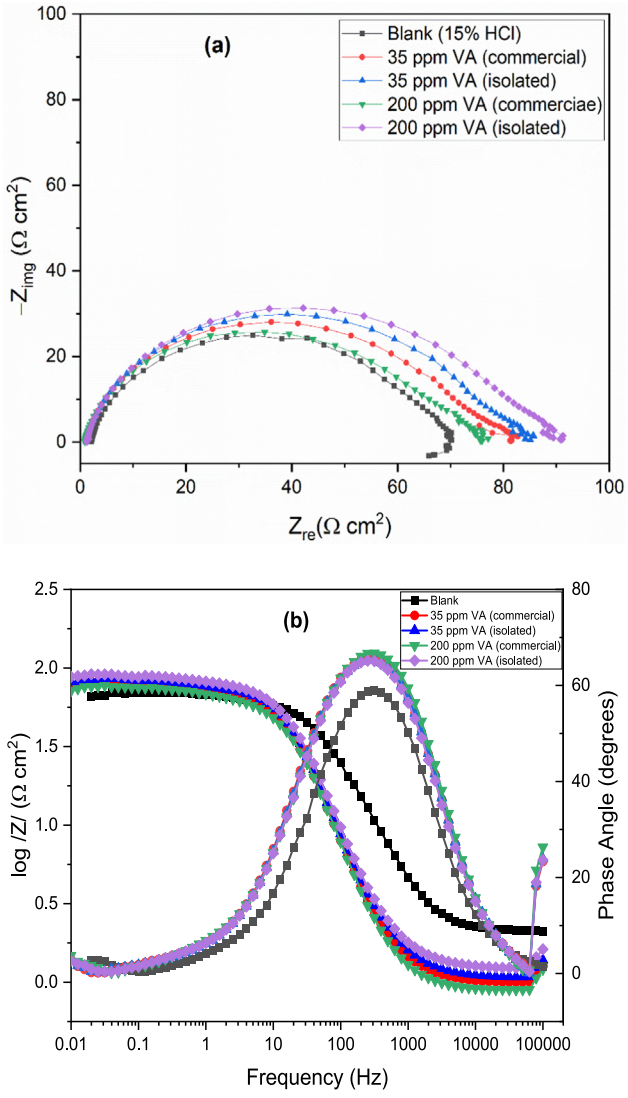

Fig. 5. Impedance plots for X60 carbon steel in 15% HCl solution without and with different concentrations of VA at 25 °C in (a) Nyquist and (b) Bode plots.

loss experiment was undertaken at 25 and 60 °C using different concentrations (50 and 200 ppm) of OA and 200 ppm of VA isolates. Weight loss experiments were performed using X60 carbon steel coupons cut into 1.70 cm × 1.70 cm × 1.10 cm dimensions with total surface areas of 13.26 cm^2. The calculated values of weight loss (obtained from the difference in weight of the coupons after and before immersion for 24 h), corrosion rate and inhibition efficiency for X60 steel in 15% HCl without and with different isolates (OA and VA) at different temperatures (25 and 60 °C) are listed in Table 3. Corrosion rate, surface coverage, and inhibition efficiency were computed using the equations (1), (2), and (3) respectively.

It is clear from the table that weight loss and corrosion rate of X60 steel were reduced on the introduction of both isolates into the corrosive medium indicating corrosion inhibition effect of the steel specimen in the presence of the isolates. It is also observed that corrosion rate increased with increase in temperature both in the absence and presence of the isolates. Examination of the table also revealed that the surface coverage (θ) and inhibition efficiency (IE) increased with increase in concentration of the OA and decreased with increase in temperature from 25 °C to 60 °C. The increase in the surface coverage and inhibition efficiency and the decrease in corrosion rates with the increase in concentration of OA could be ascribed to the adsorption of the molecule on the surface of steel and thus covered a certain area of the exposed electrode in HCl solution [45,46]. By increasing the inhibitor concentration, the surface coverage was greatly increased due to the availability of more inhibitor molecules to be adsorbed on its surface. On the other hand, it is noted for VA that θ and IE decreased with increase in temperature for the isolated VA while increase in IE with increase in temperature is observed for the commercial VA. The influence of impurities cannot be ruled out for the observed decrease in IE with increase in temperature for the isolated VA. It is known generally that for commercially available VA, solubility increases with increasing temperature. It is therefore not surprising that for the commercial VA, θ and IE increased with increase in temperature because its enhanced solubility by virtue of temperature rise ensures that more VA molecules are available in the corrosive medium that are adsorbed on the metal surface. This is advantageous as commercially available VA can be exploited as high temperature corrosion inhibitor.

3.3. Surface analysis

Fig. 7 exhibits surface morphology features of (a) the polished X60 steel, the steel specimen immersed in 15% HCl solution without the isolates at (b) 25 °C and (c) 60 °C and the steel specimen immersed in 15% HCl solution at 25 °C containing (d) 200 ppm OA, (e) 200 ppm VA (isolated) and (f) containing VA (commercial) at 60 °C. The steel surface is seen to be very smooth and free of any noticeable defect in the polished state. However, in the blank solutions the steel samples are observed to uniformly corrode severely with the extent of the surface damage due to corrosion as expected more pronounced at 60 °C. A heap of loosely adhered corrosion products with a salt-like appearance is observed on the surface (Fig. 7(b and c)). It has been shown in earlier studies that iron chloride salt is one of the products during the corrosion of carbon steel in HCl environment [24]. On the other hand, in the presence of OA and VA (Fig. 7 d, e and f), the X60 steel surface is relatively smooth

Table 1c
EIS parameters obtained during acid corrosion of X60 carbon steel in 15% HCl solution without and with different concentrations of commercial and isolated Vanillyl Alcohol (VA) at 25 °C.

Conc. (ppm)	R_s (Ω cm^2)	CPE_{dl}		R_{ct} (Ω cm^2)	CPE_f		R_f (Ω cm^2)	$R_p = (R_f + R_{ct})$ (Ω cm^2)	C_{dl} (μFcm^{-2})	$x^2(\times10^{-4})$	%IE
		Y_{dl} (μFcm^{-2} s^{n-1})	n_{dl}		Y_f (μF cm^{-2} s^{n-1})	n_f					
Blank	1.54	277.6	0.86	46.90	8624.0	0.89	6.94	53.84	78.1	3.38	–
35 (commercial)	1.08	61.49	1.00	78.84	430.2	0.62	6.37	85.21	61.5	87.8	36.81
35 (isolated)	1.17	55.23	1.00	82.21	351.0	0.64	6.49	88.70	55.2	90.4	39.30
200 (commercial)	0.98	66.38	1.00	74.22	511.8	0.59	8.08	82.30	66.4	125.9	34.58
200 (isolated)	1.34	51.81	1.00	87.82	359.7	0.62	6.99	94.81	51.8	95.5	43.21

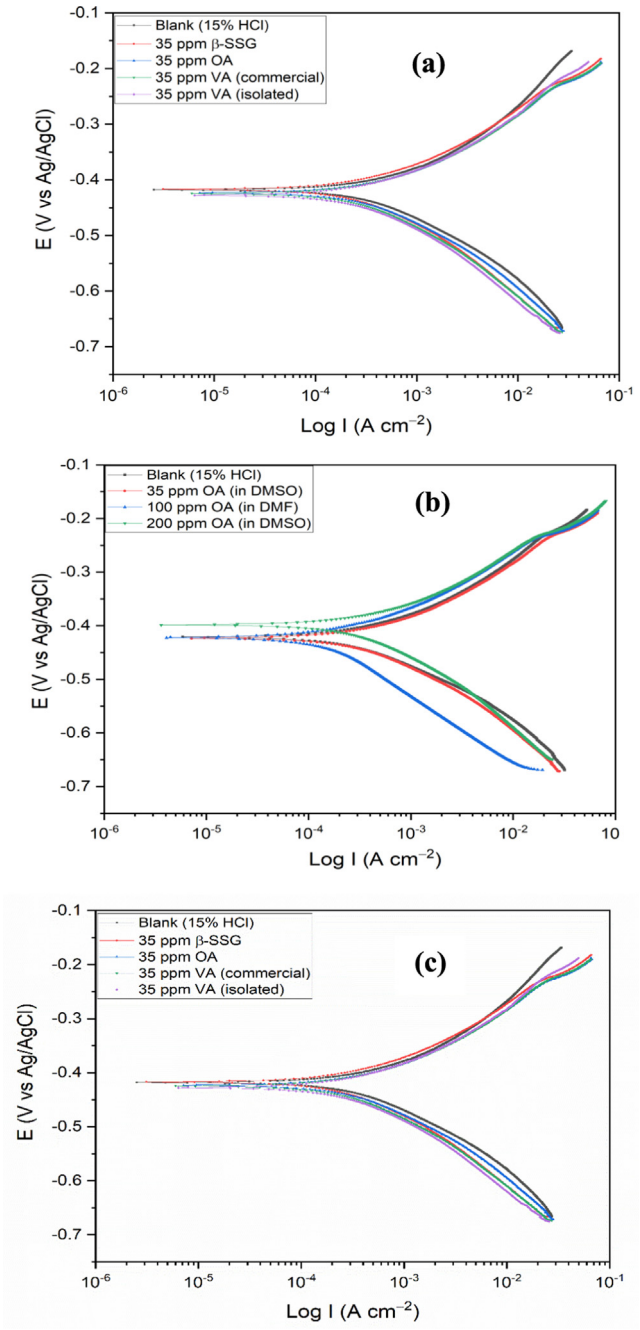

Fig. 6. Potentiodynamic polarization plots for X60 carbon steel in 15% HCl solution without and with different (a) isolates, (b) concentrations of OA and (c) VA at 25 °C.

and the corrosion grooves appear to be small compared to the blank solution. This can be attributed to a barrier layer formed between the metal and the corrosive environment, which successfully inhibits the dissolution reaction.

The composition of X60 steel surface after mechanical abrasion is shown in Fig. 8(a). The main elements are Fe (91.6%), C (7.0%), Mn (1.2%), and Si (0.3%). Fig. 8(b-f) shows the composition of the corrosion products/inhibited film deposited on the entire surface of X60 steel after immersion in 15% HCl solution without and with isolates. The EDAX results in Fig. 8(b & c) confirms the presence of Cl (7.5% at 25 °C and 19.1% at 60 °C) and O (1.4% at 25 °C and 9.9% at 60 °C) on the carbon steel surfaces which is in agreement with previous studies [47,48] where $FeCl_3$, FeO, and Fe_2O_3 were identified as the main components of the corrosion product on carbon steel surface in HCl solution. The Cl content of 19.1% at 60 °C in Fig. 8(c) is significantly reduced to 0.6% in Fig. 8(d), 1.6% in Fig. 8 (e), and 10.9% in Fig. 8(f) suggesting less corrosion probably due to adsorption of the molecules of the isolates on the steel surface. It is also noteworthy to mention that some elements like Mn was not detected on the inhibited surfaces in Fig. 8(e & f). This may be due to the covering of the metal surface by dense adsorbed inhibitor molecules. In Fig. 8(f) additional element S (4.9%) is seen and is likely coming from the DMSO used to dissolved the isolate VA before introduction into the corrosive medium.

The surface roughness of the exposed area of the steel coupons immersed in the solution without and with isolates was measured using a 3D optical profilometer (Contour GT-K, Bruker Nano GmBH, Germany). Fig. 9 presents the 3D profilometer images and reveals the surface texture and profile of the exposed areas. It is seen that the coupons immersed in the solution without the isolates at both 25 and 60 °C experienced very high surface damage as seen from Fig. 9(b) and (c), respectively as compared to the as-polished coupon (Fig. 9(a)). However, the coupons immersed in the solution containing 200 ppm of the isolates OV and VA at 25 °C showed much lesser surface damage in comparison, as shown in Fig. 9(d) and (e), respectively. The performance of the VA isolate however drops at higher temperature of 60 °C (Fig. 9(f)). The average roughness parameters for the arithmetic mean (R_A), root-mean-square (R_{RMS}) and the maximum peak-to-minimum valley (R_T) values, otherwise referred to as surface roughness parameters, and are used to quantitatively estimate surface damage are presented in Table 4. Higher surface roughness parameters indicate a higher surface damage due to corrosion. Thus, the coupons immersed in the solution without the isolates demonstrated a very high R_A, R_{RMS} and R_T values at 25 °C, about three times higher than that of the as-polished coupon, and when evaluated at elevated temperature of 60 °C, all the roughness parameters increased much higher indicating an increased damage due to corrosion. With the introduction of the OV and VA isolates at a concentration of 200 ppm, the arithmetic mean (R_A) can be seen to reduce from a value 0.84 μm (R_A of blank at 25 °C) to 0.30 and 0.69 μm (equivalent to 64 and 18%

Table 2
PDP parameters obtained during acid corrosion of X60 carbon steel in 15% HCl solution without and with different concentrations of isolated compounds at 25 °C.

System/concentration	$-E_{corr}$ (mV/Ag/AgCl)	i_{corr} (μA cm^{-2})	β_a (mV dec^{-1})	$-\beta_c$ (mV dec^{-1})	f_a	f_c	%IE
Blank	418.0	514.85	106.8	123.8	–	–	–
35 ppm β-SSG	417.6	277.2	78.9	109.2	0.54	0.54	46.16
35 ppm OA	423.5	335.2	77.2	108.3	0.70	0.62	34.89
100 ppm OA (DMF)	422,1	172.6	65.9	150.7	0.36	0.33	66.48
200 ppm OA (DMSO)	398.9	297.5	70.6	150.5	0.44	0.66	42.23
35 ppm VA (commercial)	425.5	304.2	74.1	113.5	0.65	0.55	40.91
200 ppm VA (commercial)	417	301.2	67.9	101.5	0.58	0.59	41.49
35 ppm VA (isolated)	427	278.6	75.6	107.2	0.61	0.50	45.88
200 ppm VA (isolated)	422.9	272.7	74.3	101.0	0.57	0.50	47.03

Table 3
Calculated values of weight loss, corrosion rate and inhibition efficiency for X60 steel in 15% HCl without and with isolates (OA and VA) at different temperatures for 24 h immersion.

System/Concentration	Weight loss (g)		Corrosion rate (mm/yr)		θ		%IE	
	25 °C	60 °C	25 °C	60 °C	25 °C	60 °C	25 °C	60 °C
Blank (15% HCl)	0.1074	1.9997	3.7565	69.9422	–	–	–	–
50 ppm OA	0.0703	1.3255	2.4588	46.3612	0.35	0.34	34.5	33.7
200 ppm OA	0.0501	1.2469	1.7523	43.6120	0.53	0.38	53.4	37.6
200 ppm VA (isolated)	0.0616	1.2300	2.1545	43.0209	0.43	0.39	42.6	38.5
200 ppm (commercial)	0.0698	0.9973	2.4413	34.8819	0.35	0.51	35.0	51.3

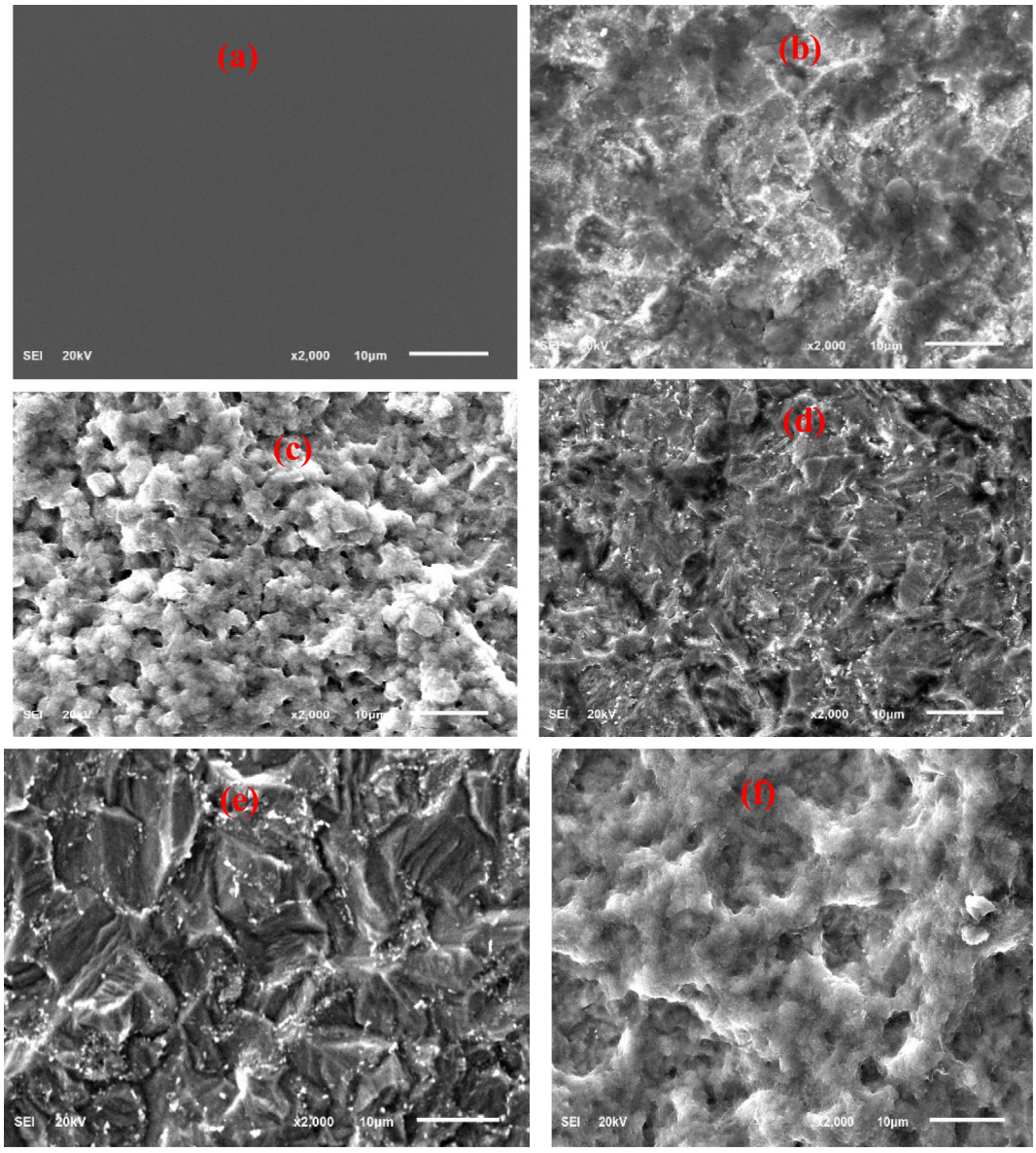

Fig. 7. SEM Surface morphology of (a) the polished X60 steel, the steel specimen immersed in 15% HCl solution without the isolates at (b) 25 °C and (c) 60 °C and the steel specimen immersed in 15% HCl solution at 25 °C containing (d) 200 ppm OA, (e) 200 ppm VA (isolated) and (f) containing VA (commercial) at 60 °C.

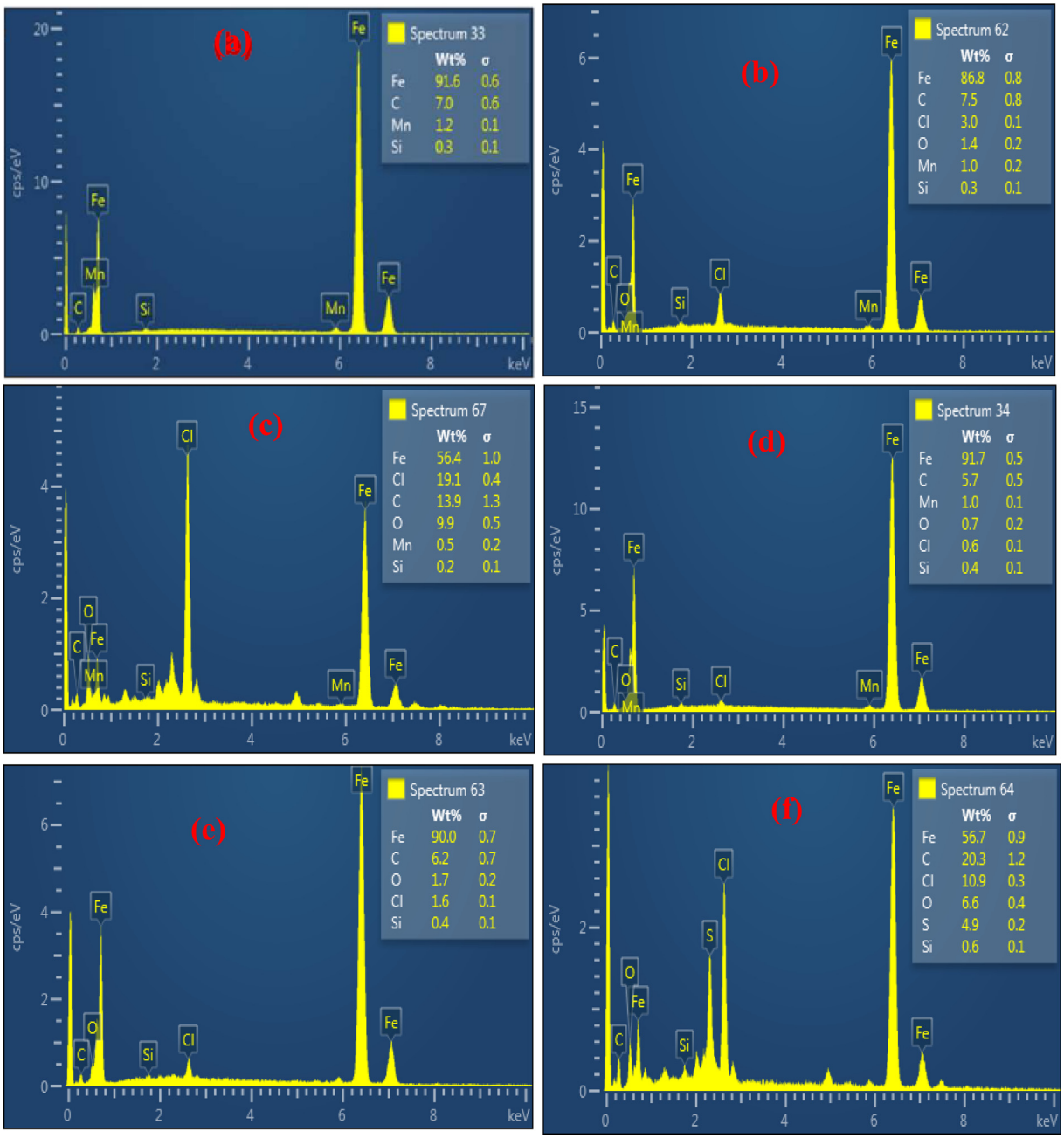

Fig. 8. EDAX spectra of (a) the polished X60 steel, the steel specimen immersed in 15% HCl solution without the isolates at (b) 25 °C and (c) 60 °C and the steel specimen immersed in 15% HCl solution at 25 °C containing (d) 200 ppm OA, (e) 200 ppm VA (isolated) and (f) containing VA (commercial) at 60 °C.

reduction), respectively. Similarly, other roughness parameters were reduced accordingly. This indicate the inhibitive performance of the isolates OV and VA at the lower temperature of 25 °C. Furthermore, the VA isolate exhibited some degree of inhibitive behavior at elevated temperature of 60 °C over the solution without the isolate. This deductible from roughness parameters (Table 4), the R_A, R_{RMS} and R_T were reduced from 2.0, 2.5 and 27 μm (for the blank at 60 °C) to 1.5, 1.90 and 20 μm (equivalent to 25, 60 and 26% reduction), respectively. Based on the R_A, which is the widely used parameters for the surface roughness estimation, the OA isolate can be deemed to be more protective and exhibit higher inhibitive characteristics as compared to the VA isolate and perhaps if used at elevated temperature (60 °C) it will outperform the VA isolate.

3.4. Theoretical studies

3.4.1. Density functional theory (DFT) calculations results

The frontier molecular orbitals are sites for reactivities and bonding involving corrosion inhibitors [30]. It has been reported

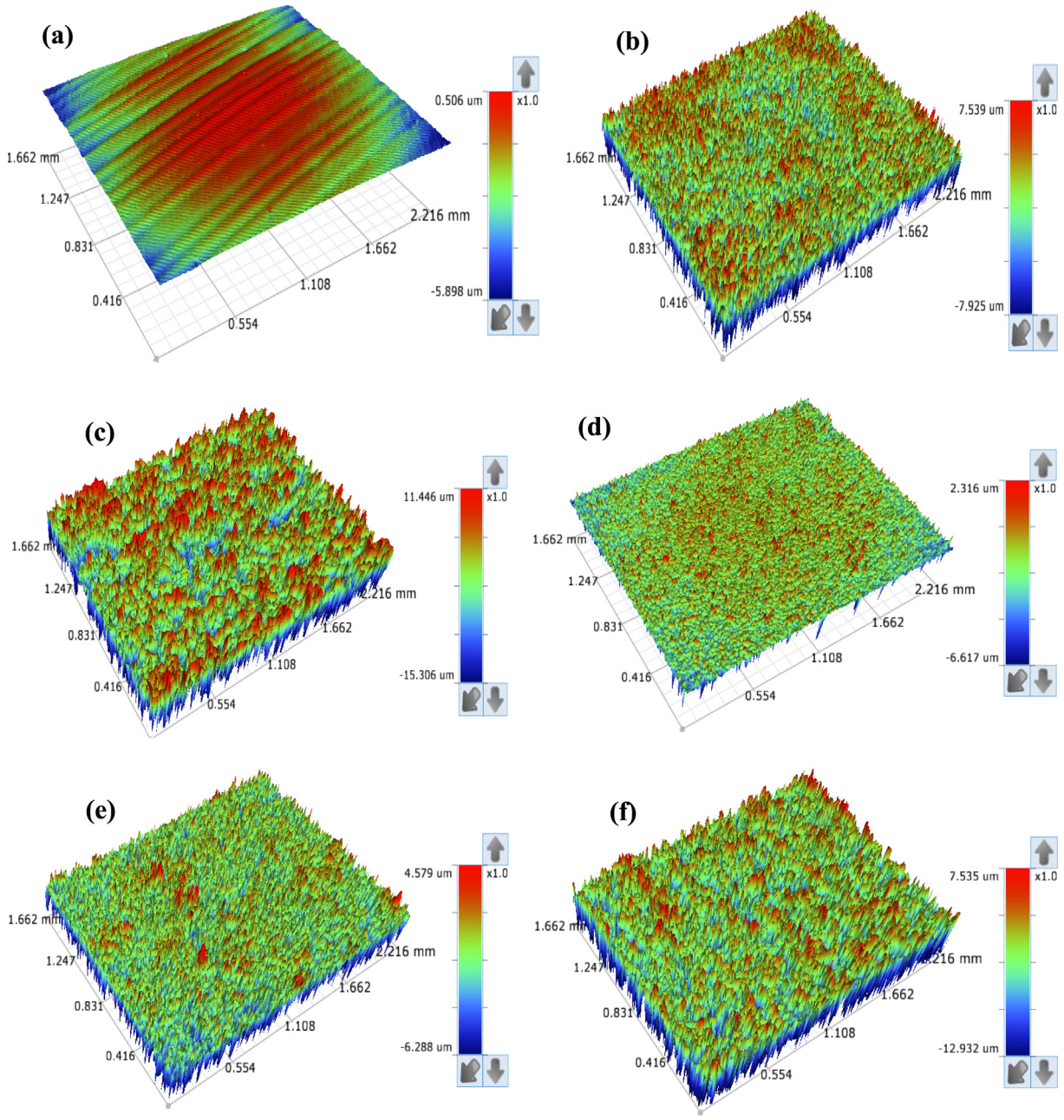

Fig. 9. Surface profilometer images of (a) the polished X60 steel, the steel specimen immersed in 15% HCl solution without the isolates at (b) 25 °C and (c) 60 °C and the steel specimen immersed in 15% HCl solution at 25 °C containing (d) 200 ppm OA, (e) 200 ppm VA (isolated) and (f) containing VA (commercial) at 60 °C.

Table 4
Surface parameters derived from profilometer surface analysis of the corroded X60 Steel immersed in 15% HCl without and with isolated compounds.

Systems/concentration	Surface Roughness		
	R_A (μm)	R_{RMS} (μm)	R_T (μm)
Polished X60 steel	0.110	0.137	6.403
X60 steel in blank at 25 °C	0.838	1.052	15.464
X60 steel in blank at 60 °C	2.021	2.529	26.752
X60 steel inhibited with 200 ppm OA at 25 °C	0.302	0.389	8.933
X60 steel inhibited with 200 ppm VA at 25 °C	0.685	0.863	10.868
X60 steel inhibited with 200 ppm VA at 60 °C	1.472	1.885	20.467

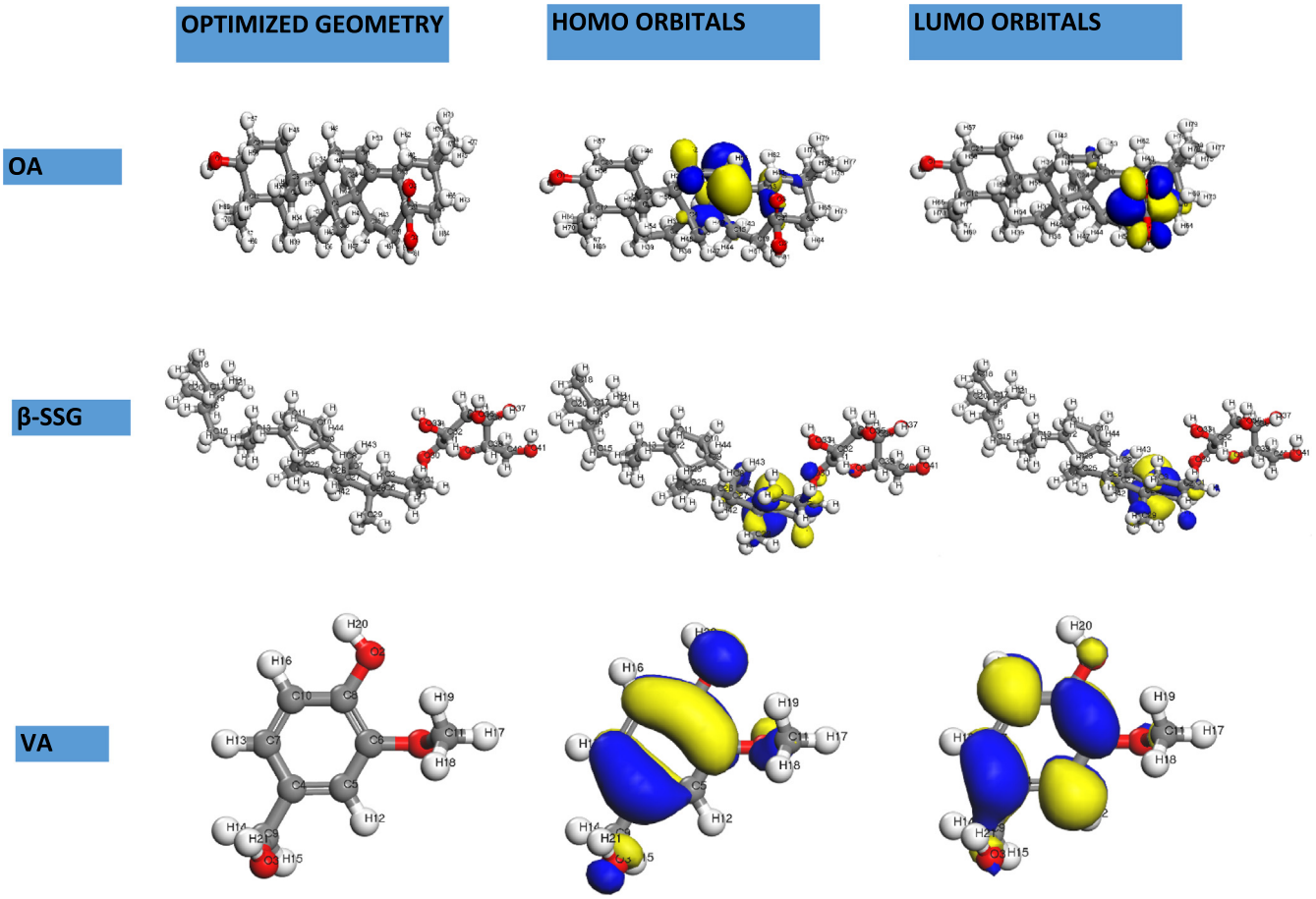

Fig. 10. Optimized geometry, HOMO and LUMO orbitals for OA, β-SSG and VA in aqueous phase using DFT at GGA/BLYP/DNP level of theory.

that the HOMO orbitals are electron donating sites while the LUMO orbitals are electron acceptor sites. Fig. 10 shows the optimized geometry, HOMO and LUMO orbitals for OA, β-SSG and VA in aqueous phase using DFT at GGA/BLYP/DNP level of theory. Results obtained from Fig. 10, shows that the HOMO orbitals are located around the bicyclic rings containing a double bond on OA and β-SSG, respectively. However, for VA, the HOMO orbital is spread over the entire molecule. This shows electron donating centers of the molecules. On the other hand, the LUMO orbitals is located on the –COOH group for OA, the bicyclic rings containing a double bond for β-SSG, and over the entire molecule for VA. The DFT results shows that the different molecules have different electrons donor and acceptor sites. This also explains the different corrosion inhibition efficiencies obtained from the three (3) isolated molecules from date palm leaves, i.e β-SSG (46.57%) > $VA_{isolated}$ (39.30%) > $VA_{commercial}$ (36.81%) > OA (31.94%) at 25 °C.

3.4.2. Monte Carlo simulation results

Monte Carlo simulations was adopted to investigate the interaction between the three isolated corrosion inhibitors from date palm leaves namely OA, β-SSG and VA on Fe (1 1 0)/200 H_2O interface. Fig. 11 shows the stable equilibrium adsorption configuration of (a) OA and (b) β-SSG and (c) VA on Fe (1 1 0)/200 H_2O interface using Monte Carlo simulation. As is seen from Fig. 11, all the inhibitors adsorbed at a parallel position on the Fe surface so as to maximize surface contact and enhance surface coverage. However, β-SSG covered more of the Fe surface. This may lead to higher inhibition of β-SSG compared to OA and VA. The adsorption energies of the inhibitors on iron surface in the presence of water obtained from Monte Carlo simulations as presented in Table 5, follows the order β-SSG > OA > VA. β-SSG is predicted to be the best corrosion inhibitor. However, the experimental inhibition efficiency obtained is as follows β-SSG > VA > OA at the lowest concentration (35 ppm) studied. However, at optimum concentration (200 ppm) studied, OA has higher efficiency than VA which is in agreement with the theoretical prediction. In both predicted and experimental results β-SSG is the best corrosion inhibitor. High negative adsorption energy indicates the system with the most stable and stronger adsorption [30,29]. The difference in inhibition efficiency between OA and VA may be due to the molecular geometry of OA and VA. VA is a flat and has all the surface molecule covered by electrons delocalization as seen in the HOMO and LUMO orbitals. This electron density makes VA able to donate more electrons to the d-orbital of the Fe surface and more stable on the Fe surface. On the other hand, OA has highly flexible and twisted structures and the electron density is not spread over the entire surface. This can lead to the low inhibition efficiency obtained. In all cases, the adsorption energies of the inhibitors are far higher than that of water molecules as evident in Table 5.

4. Conclusions

Based on the findings of the study, the following conclusions could be drawn:

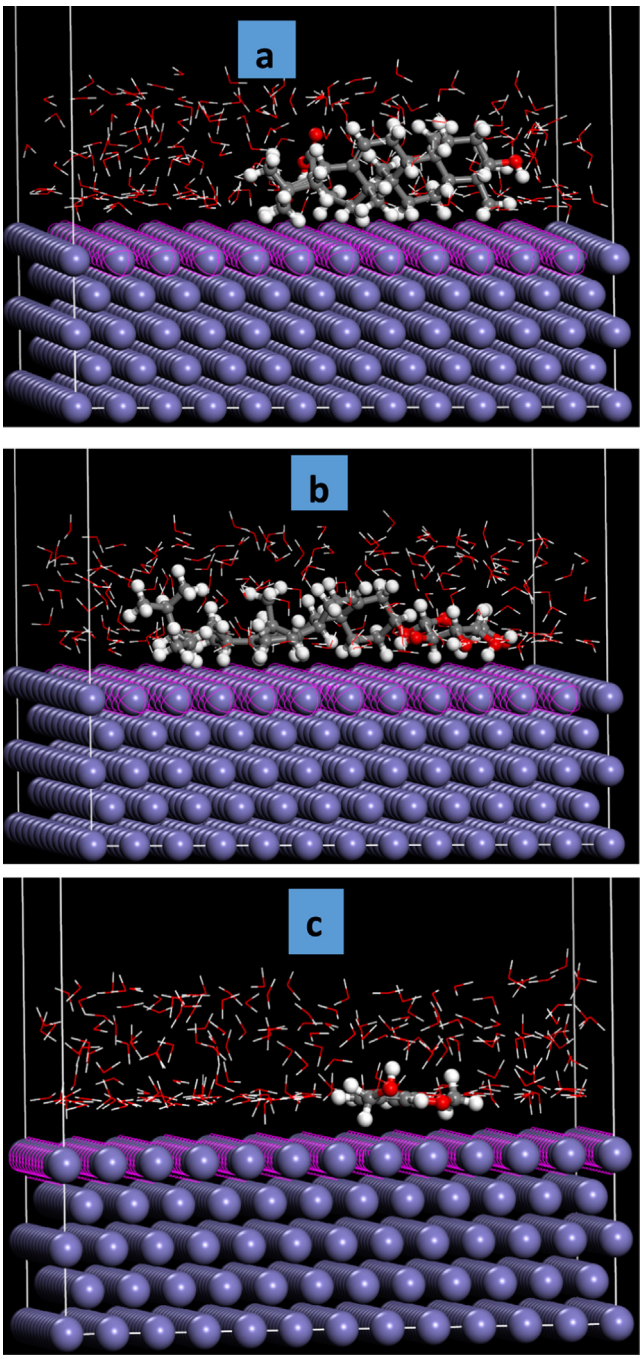

Fig. 11. Stable equilibrium adsorption configuration of (a) OA and (b) β-SSG and (c) VA on Fe (1 1 0)/200 H_2O interface using Monte Carlo simulation.

Table 5
Outputs of the Monte Carlo simulation for the lowest adsorption configurations of OA, β-SSG and VA on Fe (1 1 0)/200 H_2O Interface (in kcal mol^{-1}).

Systems	Total energy	Adsorption energy	Adsorption energy:H_2O
OA/Fe (1 1 0)	−2812.70	−205.93	−13.35
β-SSG/Fe (1 1 0)	−2860.15	−292.61	−10.91
VA/Fe (1 1 0)	−2801.92	−122.26	−13.85

1. In this work, six compounds namely oleanolic acid (OA), Vanillyl alcohol (VA), β-Sitosterol-3-O-β-D-glucoside (β-SSG), mixture of fatty alkanes (C12-C16), carotenoid lutein and sucrose sugar were isolated from butanol extract of date palm leaves.
2. Three of the compounds namely oleanolic acid (OA), vanillyl alcohol (VA), β-Sitosterol-3-O-β-D-glucoside (β-SSG) were tested as corrosion inhibitor for X60 steel in 15% HCl at 25 and 60 °C. Results show that the tested compounds exhibit moderate inhibition effect in the order β-SSG (46.6%) > VA (39.3%) > OA (31.9%) at 35 ppm concentration from EIS measurements.
3. Inhibition performance of the isolates increases with increase in concentration with 200 ppm OA performing better than 200 ppm VA. The performance of OA is influenced by organic solvent used to aid solubility in the corrosive medium. DMF is a better solvent for OA than DMSO.
4. Inhibition efficiency of the isolates slightly decreased with increase in temperature but increased for commercial VA suggesting possible influence of impurities on the performance of the studied isolates.
5. Surface analysis of the corroded steel samples without and with the isolates using 3D optical profilometer also confirm the corrosion inhibition effect of the isolates as the surface roughness parameters were reduced in the presence of the isolates compared to the blank.
6. Theoretical and experimental results are in good agreement. The adsorption energies from Monte Carlo simulation follows the order β-SSG > OA > VA. β-SSG is predicted to be the best corrosion inhibitor which was confirmed experimentally.

Declaration of Competing Interest

The authors declare that they have no known competing financial interests or personal relationships that could have appeared to influence the work reported in this paper.

Acknowledgments

Authors acknowledge the support received from King Abdul-Aziz City for Science and Technology (KACST) for funding this work under the National Science Technology Plan (NSTIP) grant No. 14-ADV2452-04. The support provided by the Deanship of Research Oversight and Coordination (DROC) and the Interdisciplinary Research Center for Advanced Materials (IRC-AM) at King Fahd University of Petroleum and Minerals (KFUPM) is also acknowledged.

References

[1] G. Koch, J. Varney, N. Thopson, O. Moghissi, M. Gould, J. Payer, Nace Int. (2016) 1–216.
[2] A.E. Miralrio, A. Vázquez, Processes 8 (2020) 942, https://doi.org/10.3390/pr8080942.
[3] C. Verma, E.E. Ebenso, I. Bahadur, M.A. Quraishi, J. Mol. Liq. (2018) 577–590, https://doi.org/10.1016/j.molliq.2018.06.110.
[4] S.A. Umoren, M.M. Solomon, I.B. Obot, R.K. Suleiman, J. Ind. Eng. Chem. 76 (2019) 91–115, https://doi.org/10.1016/j.jiec.2019.03.057.
[5] A. Thakur, A. Kumar, J. Bio-Tribo-Corrosion 7 (2) (2021) 1–48, https://doi.org/10.1007/S40735-021-00501-Y.
[6] S. Bashir, A. Thakur, H. Lgaz, I.M. Chung, A. Kumar, Arab. J. Sci. Eng. 45 (6) (2020) 4773–4783, https://doi.org/10.1007/S13369-020-04514-6.
[7] S. Bashir, A. Thakur, H. Lgaz, I.M. Chung, A. Kumar, Surf. Interfaces 20 (2020) 100542, https://doi.org/10.1016/J.SURFIN.2020.100542.
[8] S. Bashir, A. Thakur, H. Lgaz, I.M. Chung, A. Kumar, J. Mol. Liq. 293 (2019) 111539, https://doi.org/10.1016/J.MOLLIQ.2019.111539.
[9] S. Sharma, R. Ganjoo, S. Kr. Saha, N. Kang, A. Thakur, H. Assad, A. Kumar, J. Mol. Liq. 347 (2022) 118383, https://doi.org/10.1016/J.MOLLIQ.2021.118383.
[10] H. Assad, A. Kumar, J. Mol. Liq. 344 (2021) 117755, https://doi.org/10.1016/J.MOLLIQ.2021.117755.
[11] E.E. Oguzie, K.L. Oguzie, C.O. Akalezi, I.O. Udeze, J.N. Ogbulie, V.O. Njoku, ACS Sustain. Chem. Eng. 1 (2) (2012) 214–225, https://doi.org/10.1021/SC300145K.
[12] I. Radojčić, K. Berković, S. Kovač, J. Vorkapić-Furač, Corros. Sci. 50 (5) (2008) 1498–1504, https://doi.org/10.1016/J.CORSCI.2008.01.013.
[13] S. Garai, S. Garai, P. Jaisankar, J.K. Singh, A. Elango, Corros. Sci. 60 (2012) 193–204, https://doi.org/10.1016/J.CORSCI.2012.03.036.

[14] X. Li, S. Deng, H. Fu, X. Xie, Corros. Sci. 78 (2014) 29–42, https://doi.org/10.1016/J.CORSCI.2013.08.025.
[15] P.B. Raja, A.K. Qureshi, A. Abdul Rahim, H. Osman, K. Awang, Corros. Sci. 69 (2013) 292–301, https://doi.org/10.1016/J.CORSCI.2012.11.042.
[16] M. Behpour, S.M. Ghoreishi, M. Khayatkashani, N. Soltani, Mater. Chem. Phys. 131 (3) (2012) 621–633, https://doi.org/10.1016/J.MATCHEMPHYS.2011.10.027.
[17] C. Kamal, M.G. Sethuraman, Ind. Eng. Chem. Res. 51 (31) (2012) 10399–10407, https://doi.org/10.1021/IE3010379/SUPPL_FILE/IE3010379_SI_001.PDF.
[18] P.B. Raja, M. Fadaeinasab, A.K. Qureshi, A.A. Rahim, H. Osman, M. Litaudon, K. Awang, Ind. Eng. Chem. Res. 52 (31) (2013) 10582–10593, https://doi.org/10.1021/IE401387S/SUPPL_FILE/IE401387S_SI_001.PDF.
[19] A. Ostovari, S.M. Hoseinieh, M. Peikari, S.R. Shadizadeh, S.J. Hashemi, Corros. Sci. 51 (9) (2009) 1935–1949, https://doi.org/10.1016/J.CORSCI.2009.05.024.
[20] M. Chevalier, F. Robert, N. Amusant, M. Traisnel, C. Roos, M. Lebrini, Electrochim. Acta 131 (2014) 96–105, https://doi.org/10.1016/J.ELECTACTA.2013.12.023.
[21] W. Emori, V.M. Bassey, H. Louis, P.C. Okonkwo, S. Zhao, K. Wei, P.C. Okafor, J. Wan, C.R. Cheng, Bioelectrochemistry 141 (2021) 107840, https://doi.org/10.1016/J.BIOELECHEM.2021.107840.
[22] S.A. Umoren, Z.M. Gasem, I.B. Obot, Anti-Corrosion Methods Mater. 62 (1) (2015) 19–28, https://doi.org/10.1108/ACMM-10-2013-1302.
[23] S.A. Umoren, M.M. Solomon, I.B. Obot, Sustainability 13 (2021) 5569.
[24] S.A. Umoren, M.M. Solomon, I.B. Obot, R.K. Suleiman, Environ. Sci. Pollut. Res. 28 (30) (2021) 40879–40894, https://doi.org/10.1007/s11356-021-13567-5.
[25] S.A. Umoren, M.M. Solomon, I.B. Obot, R.K. Suleiman, J. Adhes. Sci. Technol. 32 (17) (2018) 1934–1951, https://doi.org/10.1080/01694243.2018.1455797.
[26] I.B. Onyeachu, I.B. Obot, A.A. Sorour, M.I. Abdul-Rashid, Corros. Sci. 150 (2019) 183–193, https://doi.org/10.1016/j.corsci.2019.02.010.
[27] ASTM International, Standard Practice for Preparing, Cleaning, and Evaluating Corrosion Test, 1999.
[28] R.L.C. Akkermans, N.A. Spenley, S.H. Robertson, Mol. Simul. 39 (14–15) (2013) 1153–1164, https://doi.org/10.1080/08927022.2013.843775.
[29] P.K. Paul, M. Yadav, I.B. Obot, J. Mol. Liq. 314 (2020) 113513, https://doi.org/10.1016/j.molliq.2020.113513.
[30] L. Guo, G. Ye, I.B. Obot, X. Li, X. Shen, W. Shi, X. Zheng, Int. J. Electrochem. Sci. 12 (2017) 166–177, https://doi.org/10.20964/2017.01.04.
[31] C. Verma, L.O. Olasunkanmi, E.E. Ebenso, M.A. Quraishi, I.B. Obot, J. Phys. Chem. C 120 (21) (2016) 11598–11611, https://doi.org/10.1021/ACS.JPCC.6B04429/SUPPL_FILE/JP6B04429_SI_001.PDF.
[32] R.K. Suleiman, W. Iali, B. el Ali, S.A. Umoren, Mol. 26 (14) (2021) 4192, https://doi.org/10.3390/MOLECULES26144192.
[33] A.A. Farag, M.A. Hegazy, Corros. Sci. 74 (2013) 168–177, https://doi.org/10.1016/j.corsci.2013.04.039.
[34] H.M. Abd El-Lateef, Appl. Surf. Sci. 501 (2020), https://doi.org/10.1016/j.apsusc.2019.144237.
[35] N.A. Odewunmi, M.M. Solomon, S.A. Umoren, S.A. Ali, ACS Omega 5 (2020) 27057–27071, https://doi.org/10.1021/acsomega.0c02345.
[36] H. Boudellioua, Y. Hamlaoui, L. Tifouti, F. Pedraza, Appl. Surf. Sci. 473 (2018) 449–460, https://doi.org/10.1016/j.apsusc.2018.12.164.
[37] M.V. Fiori-bimbi, P.E. Alvarez, H. Vaca, C.A. Gervasi, Corros. Sci. 92 (2015) 192–199, https://doi.org/10.1016/j.corsci.2014.12.002.
[38] M. Palomar-Pardavé, M. Romero-Romo, H. Herrera-Hernández, M.A. Abreu-Quijano, N.V. Likhanova, J. Uruchurtu, J.M. Juárez-García, Corros. Sci. 54 (2012) 231–243.
[39] Y.T. Du, H.L. Wang, Y.R. Chen, H.P. Qi, W.F. Jiang, J. Environ. Chem. Eng. 5 (6) (2017) 5891–5901, https://doi.org/10.1016/j.jece.2017.11.004.
[40] G.J. Brug, A.L.G. van den Eeden, M. Sluyters-Rehbach, J.H. Sluyters, J. Electroanal. Chem. 176 (1–2) (1984) 275–295, https://doi.org/10.1016/S0022-0728(84)80324-1.
[41] K.W. Tan, M.J. Kassim, Corros. Sci. 53 (2) (2011) 569–574, https://doi.org/10.1016/j.corsci.2010.09.065.
[42] W. Zhang, H.J. Li, Y. Wang, Y. Liu, Q.Z. Gu, Y.C. Wu, New J. Chem. 42 (15) (2018) 12649–12665, https://doi.org/10.1039/c8nj01762j.
[43] A. Saady, Z. Rais, F. Benhiba, R. Salim, K. Ismaily Alaoui, N. Arrousse, F. Elhajjaji, M. Taleb, K. Jarmoni, Y. Kandri Rodi, I. Warad, A. Zarrouk, Corros. Sci. 189 (2021) 109621, https://doi.org/10.1016/J.CORSCI.2021.109621.
[44] P. Arellanes-Lozada, V. Díaz-Jiménez, H. Hernández-Cocoletzi, N. Nava, O. Olivares-Xometl, N.V. Likhanova, Corros. Sci. 175 (2020) 108888, https://doi.org/10.1016/j.corsci.2020.108888.
[45] R. Baskar, H. Lgaz, R. Salghi, Chem. Sci. Eng. Res. 1 (1) (2019) 32–54, https://doi.org/10.36686/ariviyal.cser.2019.01.01.005.
[46] G. Manokaran, M. Prabakaran, Chem. Sci. Eng. Res. 1 (1) (2019) 16–24, https://doi.org/10.36686/ariviyal.cser.2019.01.01.003.
[47] I.B. Obot, M.M. Solomon, I.B. Onyeachu, S.A. Umoren, A. Meroufel, A. Alenazi, A. A. Sorour, Desalination 495 (July) (2020) 114675, https://doi.org/10.1016/j.desal.2020.114675.
[48] M.M. Solomon, S.A. Umoren, M.A. Quraishi, M. Salman, J. Colloid Interface Sci. 551 (2019) 47–60, https://doi.org/10.1016/j.jcis.2019.05.004.